Magic Nature of Neutrons in ^{54}Ca: First Mass Measurements of $^{55–57}$Ca

S. Michimasa,[1,*] M. Kobayashi,[1] Y. Kiyokawa,[1] S. Ota,[1] D. S. Ahn,[2] H. Baba,[2] G. P. A. Berg,[3] M. Dozono,[1] N. Fukuda,[2] T. Furuno,[4] E. Ideguchi,[5] N. Inabe,[2] T. Kawabata,[4] S. Kawase,[6] K. Kisamori,[1] K. Kobayashi,[7] T. Kubo,[8,9] Y. Kubota,[2] C. S. Lee,[1,2] M. Matsushita,[1] H. Miya,[1] A. Mizukami,[10] H. Nagakura,[7] D. Nishimura,[11] H. Oikawa,[10] H. Sakai,[2] Y. Shimizu,[2] A. Stolz,[9] H. Suzuki,[2] M. Takaki,[1] H. Takeda,[2] S. Takeuchi,[12] H. Tokieda,[1] T. Uesaka,[2] K. Yako,[1] Y. Yamaguchi,[1] Y. Yanagisawa,[2] R. Yokoyama,[13] K. Yoshida,[2] and S. Shimoura[1]

[1]*Center for Nuclear Study, The University of Tokyo, 2-1 Hirosawa, Wako, Saitama 351-0198, Japan*
[2]*RIKEN Nishina Center for Accelerator-Based Science, 2-1 Hirosawa, Wako, Saitama 351-0198, Japan*
[3]*Department of Physics and Joint Institute for Nuclear Astrophysics, University of Notre Dame, Notre Dame, Indiana 46556, USA*
[4]*Department of Physics, Kyoto University, Kitashirakawa-Oiwake, Sakyo, Kyoto 606-8502, Japan*
[5]*Research Center for Nuclear Physics, Osaka University, 10-1 Mihogaoka, Ibaraki, Osaka 567-0047, Japan*
[6]*Department of Advanced Energy Engineering Sciences, Kyushu University, 6-1 Kasuga-koen, Kasuga, Fukuoka 816-8580, Japan*
[7]*Department of Physics, Rikkyo University, Toshima, Tokyo 171-8501, Japan*
[8]*Facility for Rare Isotope Beams, Michigan State University, 640 South Shaw Lane, East Lansing, Michigan 48824, USA*
[9]*National Superconducting Cyclotron Laboratory, Michigan State University, 640 South Shaw Lane, East Lansing, Michigan 48824, USA*
[10]*Department of Physics, Tokyo University of Science, Noda, Chiba 278-8510, Japan*
[11]*Department of Physics, Tokyo City University, Tamazutsumi 1-28-1, Setagaya-ku, Tokyo 158-8557, Japan*
[12]*Department of Physics, Tokyo Institute of Technology, Meguro, Tokyo 152-8551, Japan*
[13]*Department of Physics and Astronomy, The University of Tennessee, Knoxville, Tennessee 37996, USA*

(Received 5 January 2018; revised manuscript received 21 April 2018; published 11 July 2018)

We perform the first direct mass measurements of neutron-rich calcium isotopes beyond neutron number 34 at the RIKEN Radioactive Isotope Beam Factory by using the time-of-flight magnetic-rigidity technique. The atomic mass excesses of $^{55–57}$Ca are determined for the first time to be $-18650(160)$, $-13510(250)$, and $-7370(990)$ keV, respectively. We examine the emergence of neutron magicity at $N = 34$ based on the new atomic masses. The new masses provide experimental evidence for the appearance of a sizable energy gap between the neutron $2p_{1/2}$ and $1f_{5/2}$ orbitals in ^{54}Ca, comparable to the gap between the neutron $2p_{3/2}$ and $2p_{1/2}$ orbitals in ^{52}Ca. For the ^{56}Ca nucleus, an open-shell property in neutrons is suggested.

DOI: 10.1103/PhysRevLett.121.022506

The atomic nucleus has shell structures for both protons and neutrons with significant energy gaps occurring at particular occupation numbers. These numbers are called "magic numbers," in analogy to the shell structure of noble gases in atomic physics. The magic numbers, $N, Z = 2$, 8, 20, 28, 50, 82, and 126, suggested by Mayer and Jensen [1,2] are well established in nuclei on or near the valley of stability.

When advanced high-intensity radioactive isotope beam facilities became available, it became possible to explore properties of exotic nuclei far from the β-stability line towards the boundary of existence, called the proton and neutron drip lines. Measurements away from the valley of stability revealed that the magic numbers are not invariant in the entire nuclear chart. The properties of closed shells at $N = 8$, 20, and 28 are less distinct in the neutron-rich mass region [3–10]. On the other hand, it was reported that a new magic number emerges at $N = 16$ near the neutron drip line of oxygen isotopes [11]. Also, at $N = 32$, the occurrence of a significant subshell energy gap was experimentally demonstrated in the nuclear region from Ar to Cr nuclei [12–18].

In response to these experimental data, many theoretical studies were intensively carried out to understand these structural changes in nuclei far from β stability and to qualitatively predict the behavior of the nuclear structure near the drip line. As an important milestone, the emergence of a subshell closure at $N = 34$ remains a controversial topic. The theoretical prediction based on the strongly attractive interaction between $1f_{7/2}$ protons and $1f_{5/2}$ neutrons [19] indicates a similar migration of neutron $2p_{3/2}$, $2p_{1/2}$, and $1f_{5/2}$ single-particle levels at $N = 34$ to that observed at $N = 29$ [20]. Later, Steppenbeck *et al.* observed a high 2_1^+ excitation energy at 2043(19) keV in ^{54}Ca, suggesting that the neutrons in ^{54}Ca undergo sizable subshell closure [21]. However, discrepancies on the emergence of the $N = 34$ subshell closure in the neutron-rich Ca region remain even among the theories predicting the 2_1^+ energy of approximately 2.0 MeV [22–24].

In this Letter, we present the first mass measurements of the exotic calcium isotopes $^{55-57}$Ca, and we determine the neutron single-particle structure in neutron-rich calcium isotopes by using "filtering functions" of the atomic masses, which will be defined below, for estimating gap energies in the single-particle spectra.

The present experimental study was performed at the Radioactive Isotope Beam Factory at RIKEN, which is operated by RIKEN Nishina Center and Center for Nuclear Study, the University of Tokyo. The masses were measured directly by the time-of-flight magnetic-rigidity (TOF-$B\rho$) method [25,26] with a flight path of approximately 100 m from the BigRIPS separator [27] to the SHARAQ spectrometer [28].

Neutron-rich isotopes were produced by fragmentation of a ^{70}Zn primary beam at 345 MeV/u in a ^{9}Be target with a thickness of 2.2 g/cm^2. The fragments were separated by BigRIPS and transported in the High-resolution beam line to the SHARAQ spectrometer. A wedge degrader of 0.27 g/cm^2 was used at the BigRIPS focus $F1$ to remove the high flux of lower-Z fragments.

The beam line and SHARAQ were operated in the dispersion matching mode, which had a momentum resolution of better than 15 000 [29] at the focal plane with an intermediate dispersion. A schematic layout of the beam line with the locations of the detectors used in the experiment is shown in Fig. 1. The TOF was measured with newly developed CVD diamond detectors [30] installed at $F3$ and $S2$. The flight path length between $F3$ and $S2$ was 105 m along the central ray. The typical TOF was 540 ns. Because of the relatively low count rate of fragments at approximately 2000 particles/s, it is assured that all measurements belonged to a single particle. A slit at $F1$ was set to restrict the momentum spread of fragments to $\pm 0.5\%$. This setting was adopted to obtain broadly distributed fragments within the momentum acceptance against the energy-loss difference in the detectors, depending on their atomic numbers. We installed two low-pressure multiwire drift chambers (LP-MWDCs) [31] at focal planes both $F3$ and $S2$ to correct for the flight path differences within the acceptance on an event-by-event basis. The magnetic rigidity was determined using a delay-line parallel-plate avalanche counter (DL-PPAC) [32] located at $S0$. To determine the atomic number of the fragments, we used two silicon strip detectors (SSDs) at the focal plane $S2$. A detector system consisting of a plastic stopper, two high-purity germanium (HPGe) clover detectors [33], and a plastic veto detector was installed downstream of $S2$ to estimate the flux of isomeric states in the fragmented nuclei [34].

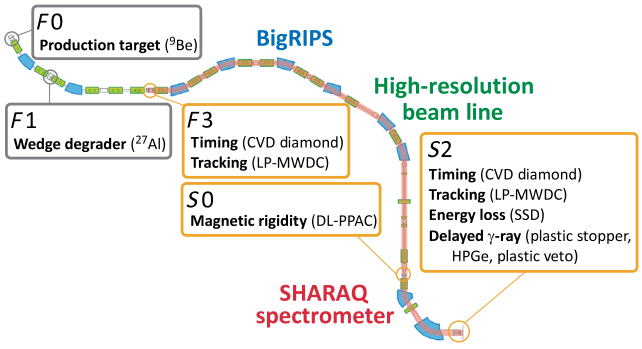

FIG. 1. Schematic layout of the detectors installed in the BigRIPS separator, the High-resolution beam line, and the SHARAQ spectrometer.

The mass of a fragment m is determined by the simultaneous measurement of charge q, TOF t, magnetic rigidity $B\rho$, and flight path length L between the timing detectors by using the equation

$$\frac{m}{q} = \frac{B\rho}{\gamma L} t = \frac{B\rho}{c} \sqrt{\left(\frac{ct}{L}\right)^2 - 1}, \tag{1}$$

where γ is the Lorentz factor. To determine nuclear masses accurately, it is crucial to determine accurately the ion-optical parameters for L and $B\rho$ from the tracking data. Since we measured $B\rho$ of the fragments at $S0$, which was located in the middle of the flight path, the TOF and beam trajectory of the fragments were affected by energy loss and multiple scattering in the DL-PPAC at $S0$. To take into account such effects, the $B\rho$ differences of the fragments relative to the central ray between $F3$ and $S0$ ($S0$ and $S2$) were tagged by the horizontal hit position at $S0$ relative to that at $F3$ ($S2$). Furthermore, the path length from $F3$ to $S0$ ($S0$ to $S2$) was also calculated precisely from the momentum vector of the beam at $F3$ ($S2$) and the $B\rho$ difference in the corresponding part. In accordance with the Taylor expansion of Eq. (1) with the hit positions and angles at both $F3$ and $S2$ and the horizontal hit position at $S0$ in addition to the TOF between $F3$ and $S2$, we considered the mass-to-charge ratio (m/q) as a fourth-order polynomial function of these observed parameters. Since this procedure took into account the transport matrix elements of the beam line up to fourth order, the atomic masses could be determined with a sufficient degree of accuracy. The coefficients of respective terms of this Taylor-expanded function were determined by a multiple polynomial regression of the ion-optical data of reference masses which were simultaneously measured in the same setting. The reference nuclei were $^{52-54}$Ca, $^{49,51-53}$K, $^{46-48}$Ar, $^{43-46}$Cl, ^{41,42}S, $^{38-42}$P, and $^{36-40}$Si [16,17,35,36], where the atomic masses were determined with precisions of better than 320 keV. Also, as reference masses, nuclei were selected only where long-lived isomeric excited states ($T_{1/2} > 100$ ns) have not been reported and were not identified by the HPGe detectors used in the present experiment because the isomeric states cause ambiguity in the mass calibration with their excitation energies.

The m/q values calibrated by the above procedure showed small shifts, depending on the atomic numbers. The previous works using the TOF-$B\rho$ method [36,37] reported the need to correct a Z dependence in the mass calibration procedure. In the present experiment, this is because the m/q spectra obtained by higher-order ion-optical corrections involve higher-order moments of a distribution, such as skewness, linked in error distributions of the tracking detectors. Based on a Z dependence in the detectors' resolutions and higher-order aberrations of the beam line, a correlation between the shift and the atomic number of fragments was considered to be mainly quadratic. Since a reasonable correlation was phenomenologically identified in the present data, the peak shifts were corrected by using a quadratic function of Z. The correction functions for the ion optics and the Z dependence were fixed after iterative examinations using the reference masses.

Figure 2(a) shows the measured m/q spectrum of the reference masses and Ca isotopes, where the masses of underlined nuclei are newly determined in the present experiment. A root-mean-square resolution of 9.85×10^{-5} was achieved for ^{55}Ca. Figure 2(b) shows the m/q differences of the present measurement and the reported values in the AME2016 database [38]. The boxes and bars show statistical errors estimated in the present measurement and the errors of masses reported in AME2016, respectively. The m/q values of the reported isotopes were systematically reproduced within an error of 6.1 keV/e, which is perceived as the systematic error [25] in this measurement. The systematic error of the Z-dependence correction was estimated to be 3.3 keV/e for Ca isotopes

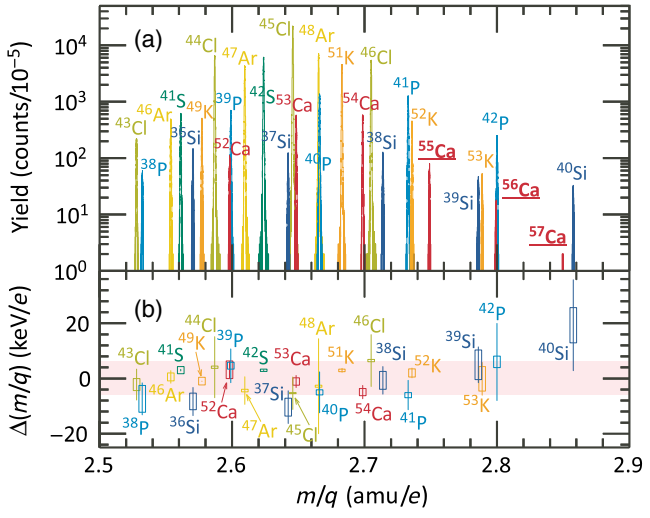

FIG. 2. (a) Measured m/q spectrum of reference masses and Ca isotopes. The underlined isotopes indicate the masses newly determined in the present experiment. (b) m/q difference between the present and the AME2016 database [38]. The boxes (bars) show statistical errors of the present measurement (the total errors in the AME2016). The red band displays the systematic error of calibration accuracy in the present measurement.

from the errors of the deduced correction function. The total errors of measured masses were attributed to those two systematic errors in addition to the statistical error.

The neutron-rich calcium isotopes yielded 3379 events for ^{55}Ca, 619 events for ^{56}Ca, and 29 events for ^{57}Ca, respectively. The atomic mass excesses of $^{55–57}$Ca were determined to be $-18\,650(160)$, $-13\,510(250)$, and $-7370(990)$ keV, respectively, as summarized in Table I. The table also shows the reference mass excesses with accuracies improved by the present measurement. The resulting values were $-22\,330(120)$ keV in ^{48}Ar, $-13\,700(110)$ keV in ^{46}Cl, $-20\,540(110)$ keV in ^{44}Cl, $+1100(100)$ keV in ^{42}P, $-8150(100)$ keV in ^{40}P, and $+5700(130)$ keV in ^{40}Si.

The two-neutron separation energies (S_{2n}) of calcium isotopes are shown in Fig. 3(a). The newly determined S_{2n} values are shown as red squares with error bars. The solid (open) circles with errors display literature (evaluation) values from the AME2016. The lines show the following theoretical predictions. MBPT [39] (solid pale rose) and IM-SRG [40] (solid green) represent advanced microscopic calculations including three-nucleon forces. KB3G [41] (dashed aqua) and modified SDPF-MU [42] (dashed red) show the results of shell model calculations by using the corresponding two-body interactions with phenomenological corrections. FRDM12 [43] (dotted burgundy), HFB24 [44] (dotted yellow), and KTUY05 [45] (dotted gray) are often-cited, global nuclear mass predictions.

Figure 3(b) shows the differences between theoretical and experimental S_{2n} values. The AME2016 evaluations for $^{55–57}$Ca are consistent with the present results, within 1σ errors. The theoretical predictions shown are distributed over several MeV. The calculations with the MBPT and KB3G interactions reproduce the present results well. The calculations by modified SDPF-MU and IM-SRG predict $^{55–57}$Ca will be loosely bound, though they provide good agreements for $^{48–54}$Ca. The FRDM12, HFB24, and KTUY05 models show a similar trend. They predict smaller values around $N = 28$ and 32 and larger values at $N = 35$ and 36.

TABLE I. The atomic mass excesses determined in the present experiment and the AME2016 database [38].

Nucleus	Present (keV)	AME2016 (keV)
^{57}Ca	−7370(990)	⋯
^{56}Ca	−13 510(250)	⋯
^{55}Ca	−18 650(160)	⋯
^{48}Ar	−22 330(120)	−22 280(310)
^{46}Cl	−13 700(110)	−13 860(210)
^{44}Cl	−20 540(110)	−20 380(140)
^{42}P	+1100(100)	+1010(310)
^{40}P	−8150(100)	−8110(150)
^{40}Si	+5700(130)	+5430(350)

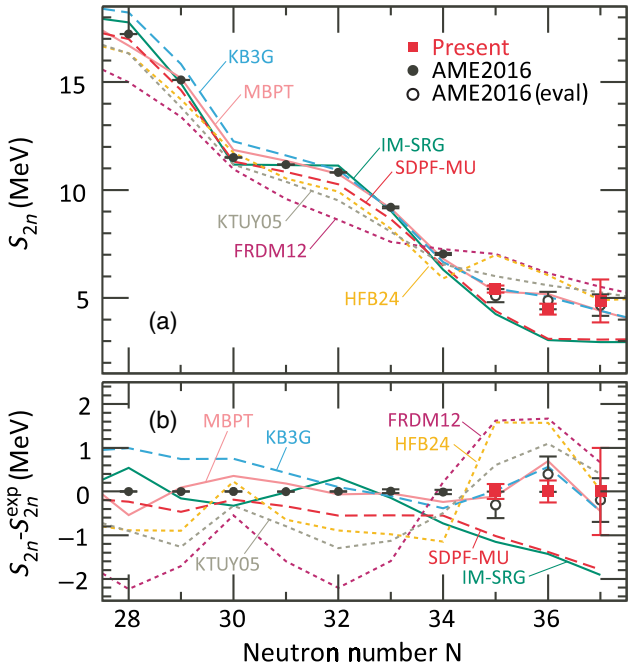

FIG. 3. (a) The two-neutron separation energies (S_{2n}) of Ca isotopes as a function of the neutron number. (b) The differences of theoretical S_{2n} from the experimental values. The symbols and lines are common in both figures. The red squares show the present results. The solid (open) circles are literature values from the AME2016 database (evaluation). The colored lines show theoretical predictions. For notations see the text.

We now discuss the magic nature at $N = 34$ in Ca isotopes based on the measured atomic masses. In a simple picture, the magic number is illustrated by an occupation number of a nucleon, at which energetically lower single-particle orbitals are completely filled and an additional nucleon settles in an upper orbital with a large energy gap. This picture of a magic number is known to be too simple in the theoretical point of view since real nucleons contained in a nucleus strongly interact with each other. Empirical indexes for evaluating the energy gap of the single-particle spectrum in nuclei [46,47] have been suggested based on experimental systematics and theoretical understanding. We describe the magic nature of Ca isotopes by using the empirical mass filters.

Satuła *et al.* [46] suggested expressing the energy gaps of single-particle spectra empirically by the following filtering function (δe) using the atomic masses of neighboring nuclei:

$$\delta e = 2[\Delta_3(N) - \Delta_3(N-1)] = S_{2n}(N) - S_{2n}(N+1), \quad (2)$$

in cases with an even N. $\Delta_3(N)$ is the three-point mass difference in a nucleus with a fixed number of protons and N neutrons and explicitly represented by

$$\Delta_3(N) = \frac{(-1)^N}{2}[M(N+1) - 2M(N) + M(N-1)], \quad (3)$$

where $M(N)$ shows the atomic mass of the nucleus with N neutrons. This quantity is known as the odd-even mass parameter of second difference [20]. It is remarkable that the Δ_3 at odd N can be associated with the pairing gap [48].

We note here the difference between δe and the empirical two-neutron shell gap $\Delta_{2n} \equiv S_{2n}(N) - S_{2n}(N+2)$ [47], which is frequently used to demonstrate a shell-gap evolution in nuclei. The Δ_{2n} shell gap closely links to the δe through the relation

$$\Delta_{2n} = 2[\delta e - \Delta_3(N+1) + \Delta_3(N-1)], \quad (4)$$

where N is an even number. Hence, the Δ_{2n} shell gap is affected by the difference of pairing gaps in the highest-occupied and lowest-open orbitals, in addition to δe. Since the pairing gaps in the $\nu(2p_{3/2})$ and $\nu(2p_{1/2})$ orbitals are known to be different in the Ca isotopes [49], the δe is considered to be better suited for the discussion on the single-particle gap in ^{54}Ca than the Δ_{2n} shell gap.

The systematic trend of the δe shell gap for neutron-rich Ca isotopes is shown in Fig. 4(a) and compared to the same

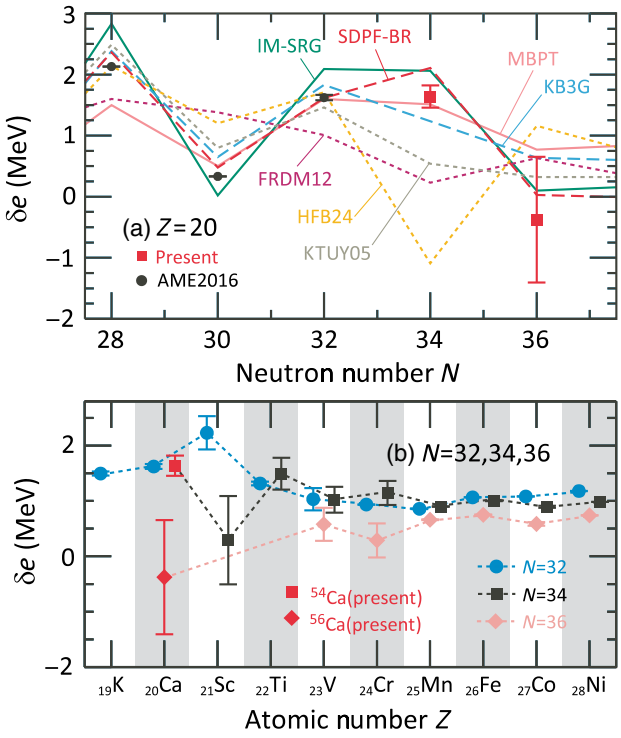

FIG. 4. Systematics of the empirical energy gaps (δe) of single-particle spectra. (a) Ca isotopes are shown with theoretical predictions. The present results are shown as red squares and the solid circles are literature values from the AME2016 database. The theoretical predictions are shown by lines with the same colors as those described in Fig. 3. (b) Isotonic chains at $N = 32$, 34, and 36 as a function of atomic number are shown. The circles, squares, and diamonds refer to $N = 32$, 34, and 36, respectively. The present results are shown as red symbols. The other values were obtained from AME2016 and Ref. [50].

theoretical predictions as shown in Fig. 3. The δe value of ^{54}Ca is comparable to that of ^{52}Ca and slightly smaller than that of ^{48}Ca. This denotes that ^{54}Ca has a magic nature of neutrons, as is the case with ^{52}Ca. The δe value of ^{56}Ca is smaller than those of ^{48,52,54}Ca, having the neutron magicity, and thus it is suggested that in ^{56}Ca occupied and unoccupied neutron orbitals are packed near the Fermi surface. The theories cannot completely reproduce the evolution of δe of Ca isotopes as a function of the neutron numbers. The KB3G calculations show a reduction of δe from $N = 32$ to 34. The MBPT calculations reproduce well the energy gaps in ^{52,54}Ca; however, the δe of ^{48}Ca is smaller than those of ^{52,54}Ca. The IM-SRG prediction reproduces the data with relatively good accuracy in this region, but its variation is slightly larger than in the experiment.

Figure 4(b) shows the δe shell gaps for $N = 34$ (square) and 36 (diamond) as a function of the atomic number in comparison with $N = 32$ (circle). The present values are shown as red symbols. The other values were obtained from the AME2016 database and the newly reported masses in $^{52-55}$Ti isotopes [50]. Along the $N = 32$ and 34 chains, the δe values in Ca increase by approximately 1.5 times compared to the constant values around $Z = 25$ (Mn). However, the small δe in ^{55}Sc and the large δe in ^{53}Sc suggest that in Sc isotopes the $N = 32$ energy gap emerges, but there is no gap at $N = 34$. Therefore, it is suggested that the energy difference between the $\nu(2p_{1/2})$ and $\nu(1f_{5/2})$ orbitals becomes large from Sc to Ca. Meanwhile, the δe values at $N = 36$ are small across $Z = 20$–28, and comparable to the δe of the $N = 30$ isotope, ^{50}Ca [see Fig. 4(a)]. Therefore, it is suggested that ^{56}Ca has an open-shell character for neutrons similar to other $N = 36$ isotones. This is reasonably interpreted using a picture in which the valence neutrons partly fill the $1f_{5/2}$ orbital beyond the $N = 34$ gap.

In conclusion, the atomic masses of the neutron-rich calcium isotopes $^{55-57}$Ca were measured by using the TOF-$B\rho$ method and determined for the first time. By observation of the mass evolution in Ca isotopes beyond $N = 34$, the magic nature at $N = 34$ in the neutron-rich Ca region became evident. The energy gap of the single-neutron spectrum in ^{54}Ca was evaluated to be comparable with that in ^{52}Ca based on the experimental δe shell gaps. Also, it was experimentally shown that the energy gaps of single-neutron spectra in the $N = 34$ isotones become significant from Sc to Ca. The δe shell gap in ^{56}Ca suggests an open-shell character for neutrons. The δe values in ^{54,56}Ca indicate that the closure of the $\nu(2p_{1/2})$ orbital causes the magicity at $N = 34$.

We thank the RIKEN Nishina Center and the Center for Nuclear Study, the University of Tokyo accelerator staff for the excellent beam delivery. We also thank Professor N. Shimizu for the fruitful discussions. This work is financially supported in part by JSPS KAKENHI Grant No. JP22740150. M. K. is grateful to the JSPS for a Research Fellowship for young scientists under Program No. JP14J03376. G. P. A. B. acknowledges support from the National Science Foundation through Grant No. PHY-1068192, and the Joint Institute for Nuclear Astrophysics Center for the Evolution of the Elements through Grants No. PHY-0822648 and No. PHY-1430152.

*mitimasa@cns.s.u-tokyo.ac.jp

[1] M. G. Mayer, Phys. Rev. **75**, 1969 (1949).
[2] O. Haxel, J. H. D. Jensen, and H. E. Suess, Phys. Rev. **75**, 1766 (1949).
[3] A. Navin *et al.*, Phys. Rev. Lett. **85**, 266 (2000).
[4] H. Iwasaki *et al.*, Phys. Lett. B **481**, 7 (2000).
[5] H. Iwasaki *et al.*, Phys. Lett. B **491**, 8 (2000).
[6] S. Shimoura *et al.*, Phys. Lett. B **560**, 31 (2003).
[7] C. Thibault, R. Klapisch, C. Rigaud, A. M. Poskanzer, R. Prieels, L. Lessard, and W. Reisdorf, Phys. Rev. C **12**, 644 (1975).
[8] T. Motobayashi *et al.*, Phys. Lett. B **346**, 9 (1995).
[9] B. Bastin *et al.*, Phys. Rev. Lett. **99**, 022503 (2007).
[10] S. Takeuchi *et al.*, Phys. Rev. Lett. **109**, 182501 (2012).
[11] A. Ozawa, T. Kobayashi, T. Suzuki, K. Yoshida, and I. Tanihata, Phys. Rev. Lett. **84**, 5493 (2000).
[12] J. I. Prisciandaro *et al.*, Phys. Lett. B **510**, 17 (2001).
[13] R. V. F. Janssens *et al.*, Phys. Lett. B **546**, 55 (2002).
[14] A. Huck, G. Klotz, A. Knipper, C. Miehé, C. Richard-Serre, G. Walter, A. Poves, H. L. Ravn, and G. Marguier, Phys. Rev. C **31**, 2226 (1985).
[15] A. Gade *et al.*, Phys. Rev. C **74**, 021302(R) (2006).
[16] F. Wienholtz *et al.*, Nature (London) **498**, 346 (2013).
[17] M. Rosenbusch *et al.*, Phys. Rev. Lett. **114**, 202501 (2015).
[18] D. Steppenbeck *et al.*, Phys. Rev. Lett. **114**, 252501 (2015).
[19] T. Otsuka, R. Fujimoto, Y. Utsuno, B. A. Brown, M. Honma, and T. Mizusaki, Phys. Rev. Lett. **87**, 082502 (2001).
[20] A. Bohr and B. R. Mottelson, *Nuclear Structure*, Vol. I (World Scientific, Singapore, 1988).
[21] D. Steppenbeck *et al.*, Nature (London) **502**, 207 (2013).
[22] L. Coraggio, A. Covello, A. Gargano, and N. Itaco, Phys. Rev. C **80**, 044311 (2009).
[23] T. Otsuka, T. Suzuki, J. D. Holt, A. Schwenk, and Y. Akaishi, Phys. Rev. Lett. **105**, 032501 (2010).
[24] G. Hagen, M. Hjorth-Jensen, G. R. Jansen, R. Machleidt, and T. Papenbrock, Phys. Rev. Lett. **109**, 032502 (2012).
[25] A. Gillibert *et al.*, Phys. Lett. B **176**, 317 (1986).
[26] D. J. Vieira, J. M. Wouters, K. Vaziri, R. H. Kraus, H. Wollnik, G. W. Butler, F. K. Wohn, and A. H. Wapstra, Phys. Rev. Lett. **57**, 3253 (1986).
[27] T. Kubo, Nucl. Instrum. Methods Phys. Res., Sect. B **204**, 97 (2003).
[28] T. Uesaka, S. Shimoura, and H. Sakai, Prog. Theor. Exp. Phys. **2012**, 03C007 (2012).
[29] S. Michimasa *et al.*, Nucl. Instrum. Methods Phys. Res., Sect. B **317**, 305 (2013).
[30] S. Michimasa *et al.*, Nucl. Instrum. Methods Phys. Res., Sect. B **317**, 710 (2013).
[31] H. Miya *et al.*, Nucl. Instrum. Methods Phys. Res., Sect. B **317**, 701 (2013).

[32] H. Kumagai, A. Ozawa, N. Fukuda, K. Sümmerer, and I. Tanihata, Nucl. Instrum. Methods Phys. Res., Sect. A **470**, 562 (2001).
[33] K. Hosomi *et al.*, Prog. Theor. Exp. Phys. **2015**, 081D01 (2015).
[34] S. Michimasa *et al.*, Proc. Sci., INPC2016 (**2017**) 106.
[35] M. Wang, G. Audi, A. H. Wapstra, F. G. Kondev, M. MacCormick, X. Xu, and B. Pfeiffer, Chin. Phys. C **36**, 1603 (2012).
[36] Z. Meisel *et al.*, Phys. Rev. Lett. **114**, 022501 (2015).
[37] M. Matoš *et al.*, Nucl. Instrum. Methods Phys. Res., Sect. A **696**, 171 (2012).
[38] M. Wang, G. Audi, F. G. Kondev, W. J. Huang, S. Naimi, and X. Xu, Chin. Phys. C **41**, 030003 (2017).
[39] J. D. Holt, T. Otsuka, A. Schwenk, and T. Suzuki, J. Phys. G **39**, 085111 (2012).
[40] S. R. Stroberg, A. Calci, H. Hergert, J. D. Holt, S. K. Bogner, R. Roth, and A. Schwenk, Phys. Rev. Lett. **118**, 032502 (2017).
[41] A. Poves, J. Sánchez-solano, E. Caurier, and F. Nowacki, Nucl. Phys. **A694**, 157 (2001).
[42] Y. Utsuno, T. Otsuka, B. A. Brown, M. Honma, T. Mizusaki, and N. Shimizu, Phys. Rev. C **86**, 051301 (2012).
[43] P. Möller, A. J. Sierk, T. Ichikawa, and H. Sagawa, At. Data Nucl. Data Tables **109–110**, 1 (2016).
[44] S. Goriely, N. Chamel, and J. M. Pearson, Phys. Rev. C **88**, 024308 (2013).
[45] H. Koura, T. Tachibana, M. Uno, and M. Yamada, Prog. Theor. Phys. **113**, 305 (2005).
[46] W. Satuła, J. Dobaczewski, and W. Nazarewicz, Phys. Rev. Lett. **81**, 3599 (1998).
[47] D. Lunney, J. M. Pearson, and C. Thibault, Rev. Mod. Phys. **75**, 1021 (2003).
[48] S. A. Changizi, C. Qi, and R. Wyss, Nucl. Phys. **A940**, 210 (2015).
[49] B. A. Brown, Phys. Rev. Lett. **111**, 162502 (2013).
[50] E. Leistenschneider *et al.*, Phys. Rev. Lett. **120**, 062503 (2018).